J. Astrophys. Astr. (2021) 42:99
https://doi.org/10.1007/s12036-021-09774-8

Effect of intense geomagnetic storms on low-latitude TEC during the ascending phase of the solar cycle 24

ABHA SINGH[1,2], VISHNU S. RATHORE[1], SANJAY KUMAR[1], S. S. RAO[1], SUDESH K. SINGH[2] and A. K. SINGH[1,*]

[1]Department of Physics, Institute of Science, Banaras Hindu University, Varanasi 221005, India.
[2]Department of Physics, T. D. P. G. College, Jaunpur, India.
E-mail: singhak@bhu.ac.in

MS received 11 November 2020; accepted 24 May 2021

Abstract. The results presented in this paper are obtained from low-latitude ionospheric total electron content (TEC) variation during the chosen geomagnetic storm events happening during the solar cycle 24. We include the four intense geomagnetic storms that occurred on 26 September 2011, 15 July 2012, 19 February 2014 and 20 December 2015, depending upon the availability of TEC data. For this, we have used the TEC data from low-latitude station Varanasi (geographic latitude 25°, 16′N, geographic longitude 82°, 59′E and geomagnetic latitude 16°, 24′N) and an equatorial station Bengaluru (geographic latitude 13°, 02′N, geographic longitude 77°, 34′E and geomagnetic latitude 04°, 68′N). The storm-induced TEC changes at chosen stations have been discussed in terms of local time, storm wind effect, neutral wind, composition changes and variation in the dawn–dusk component of the interplanetary electric field (IEF E_y).

Keywords. Global positioning system—total electron contents—geomagnetic storm—low latitude.

1. Introduction

Ionospheric disturbances during the geomagnetic storms are very important to study as they affect ground- and space-based technological systems (Basu *et al.* 2008; Chen *et al.* 2008; Jain *et al.* 2010). Solar active regions normally approach kilogauss values in their magnetic field. The three-dimensional topology of these sectors can favour the production of sheared arcades and flux ropes. A flux rope can develop by reconnection for which various instability and eruption physical mechanisms are accountable. The magnetic reconnection on solar arcades causes coronal mass ejection (CME). The series of closely occurring loops of magnetic lines of force are present at solar arcades having a huge amount of energy. When two oppositely directed magnetic lines of force are brought together, these lines of force reconnect into a low arcade loop leaving a helix of magnetic fields unconnected to the rest of the arcade. This results in the formation of a current sheet for which the spontaneous reconnection (Vekstein 2017) and forced magnetic reconnection (Hahm & Kulsrud 1985) are considered to be responsible. A detail of these mechanisms could be found elsewhere (Srivastava *et al.* 2019). During the reconnection process, sudden release of energy takes place as a solar flare and the unconnected helical magnetic field and the material that it contains may violently expand outwards forming a CME. The occurrence of CME increases with an increase in solar activity. Within 5 days after the eruption from the sun CMEs approach the Earth. CMEs interact with the solar wind and interplanetary magnetic field (IMF) while heading to the Earth; as a result, fast CME accelerated towards the speed of the solar wind and slow CME decelerated towards the speed of the solar wind. The fast CME drives a shock which generates geomagnetic storms that may disturb the Earth's magnetosphere. Thus, the geomagnetic storms are characterised by a temporary disruption in the Earth's magnetic field that originates from the CMEs and solar flares (Piersanti *et al.* 2017).

Published online: 23 August 2021

Geomagnetic storms produce enormous and quick changes in magnetospheric convection. Apart from CME with coronal signature, many observations also evidence a sheath CME that has no obvious low coronal signature and frequently found to be originated from quiet-Sun regions and regions close to open magnetic field (Mishra & Srivastava 2019). The impact of intense geomagnetic activity occurred due to the sheath CMEs of the August 2018 event in the total electron content (TEC) is studied by Piersanti *et al.* (2020) and they have not observed any loss of lock signal.

During the geomagnetic storm, the ionospheric response is observed either due to a change in the electric field or due to thermospheric changes. When the interplanetary geomagnetic field is either directed southward (undershielding condition) or northward from its southerly course (overshielding condition), a transient electric field is produced that reached from high to mid and then low latitude within a few minutes (Kikuchi *et al.* 1996). This field is called prompt penetration electric field that arises due to the under-shielding/over-shielding conditions, divergence of the asymmetric ring currents and enhanced polar cap potential drop (Fejer *et al.* 2007). The direction of the PP electric field during the southerly phase of IMF B_z is eastward/westward during day/night. The direction of the PP electric field gets reversed during the northward turning of IMF B_z. The convection electric field in the outer magnetosphere is described as the source of the PP electric field. These magnetospheric electric fields communicate with the ionosphere through Region 1 (R1) and Region 2 (R2) field-aligned currents (FACs). With undershielding conditions, the duskward convection electric field will penetrate the mid- and low-latitude ionosphere and remain eastward on the dayside before the R2 FAC is fully developed. With the overshielding condition, an abrupt northward turning of IMF B_z after a prolonged southward orientation may cause the R2 FAC to be stronger than the R1 FAC for a while, during which the downward shielding electric field can penetrate the equator and remain westward on the dayside. Thus, the electric field of low and equatorial ionosphere is altered by the direct prompt penetration of the dawn–dusk electric field (Sastri *et al.* 1992), which further changes the plasma distribution of the region. Since the PP electric field is in the same direction as the ambient electric field, it pushes up the $\boldsymbol{E} \times \boldsymbol{B}$ drift to higher altitudes (Rastogi & Klobuchar 1990). Because of the larger production to loss ratio at higher heights, TEC increases during sunlit hours (Tsurutani *et al.* 2004). Additionally, the PP electric field causes the intensification of latitudinal expansion of the equatorial ionization anomaly (EIA) (Veenadhari *et al.* 2010).

The high-energy depositions at high latitude during geomagnetic storm cause changes in thermospheric changes and, resultantly, the dynamics action of wind produces a disturbance dynamo electric field (DDEF). The joule heating of the thermosphere due to the auroral electrojets (AEs) are intensification sets of equatorward wind circulation (Mazaudier & Venkateswaran 1990). This equatorward plasma flow turns westward at mid-latitudes due to Coriolis force which, in combination with the downward component of the Earth's magnetic field, produces an equatorward Pedersen current. As a result, the positive charges are accumulated at the equatorial side and electrons at the poleward side. The poleward electric field, thus generated, gives rise to a large eastward Hall current and a poleward Pedersen current. This physical process is called the ionospheric disturbance dynamo (DD) (Blanc & Richmond 1980). A few hours are required for the disturbance winds and DDEF to set up (Huang 2013). The direction of DDEF is westward during the day and eastward during the night (Zhao *et al.* 2005). Contrary to this, the ambient zonal electric field is eastward during the daytime and westward during the night time. These two oppositely directed electric fields severely affect $E \times B$ plasma drift leading to redistribution of plasma in the ionosphere. The observed increase or decrease in the TEC is termed as a positive/negative storm (Buonsanto 1999). Positive or negative storm effects are dependent upon latitude, local time and phase of the storm (Pedatella *et al.* 2009). The DDEF diminishes the dynamo electric field during the daytime. This results in reduction of vertical drift and therefore depletion in TEC and concealment of EIA are observed as an effect of DDEF in the dayside sector. The DDEF is associated with enhanced energy deposition into the high-latitude ionosphere during the geo-magnetically disturbed periods (Blanc & Richmond 1980) and it takes several hours to days in ionospheric response (Scherliess & Fejer 1997; Fuller-Rowell *et al.* 2002).

Direct particle precipitation at high latitudes during the main phase of the geomagnetic storm increases the AE current. As a result, the joule heating is enhanced, which may change meridional pressure gradients. This ultimately generates the atmospheric gravity waves. During propagating meridionally away from high to equatorial low latitudes, these waves are dispersed and then behave as travelling atmospheric disturbances

(TADs; Balthazor & Moffett 1997). The combined effect of the TADs and the meridional wind cause an uplift of plasma along the geomagnetic field lines to higher altitudes and therefore the peak height of the F region is uplifted (Sastri *et al.* 2000). Bauske *et al.* (1997) have reported that the peak electron density initially decreases and then increases during the increase in the peak height of the F region.

At mid-latitudes, the positive or negative storm effects are modified according to wind and composition changes in the neutral atmosphere (Rishbeth *et al.* 1987). At low latitudes, the positive and negative storm effects in electron density variation are also affected by the storm-induced disturbances in electric field (Abdu 1997; Basu *et al.* 2001).

In the past, many studies have been reported for the effects of storm on ionosphere at high and mid-latitudes (Ding *et al.* 2008; Piersanti *et al.* 2017 and references therein) and at low latitudes (Dashora *et al.* 2009; Kumar & Singh 2011a,b; Galav *et al.* 2014a,b; Chakraborty *et al.* 2015 and references therein). Pedatella *et al.* (2009) have studied the TEC variation during the storm of 15 December 2006 over the Pacific Ocean region using multi-instrument data. Rama Rao *et al.* (2009) have studied the variation of TEC at different latitudes in the Indian sectors and the impact of geomagnetic storms on navigation systems by considering two successive storms that occurred between 8 and 12 November 2004. The seasonal and local time dependency in time lag between TEC response to geomagnetic storm is studied by Liu *et al.* (2010). Kumar *et al.* (2016) have reported that the storm-induced electric field can trigger the growth of Rayleigh–Taylor instability and consequently the development of the plasma bubble.

In this paper, four intense geomagnetic storms have been selected depending upon the availability of TEC data to study TEC variation at the low-latitude station Varanasi situated near the EIA crest region and an equatorial station Bengaluru during the ascending phase of the solar cycle 24. The chosen storms in this study occurred on 26 September 2011 ($Dst_{min} = -118$ nT), 15 July 2012 ($Dst_{min} = -139$ nT), 19 February 2014 ($Dst_{min} = -116$ nT) and 20 December 2015 ($Dst_{min} = -170$ nT).

2. Dataset

The GPS-derived TEC data for the station Varanasi were obtained using a Trimble GPS receiver installed at our department. TEC data for station Bengaluru were obtained from the IGS website. TEC is computed taking the integral of the total number of electrons along the line of sight between the satellite and the ground antenna. These TEC values are called slant TEC (STEC). The STEC along the line of sight is estimated from GPS observation data recorded in the RINEX format with a time resolution of 30 s and it contains un-differenced pseudo-range and carrier phase observations on L1 and L2 frequencies. The inherent receiver and satellite bias errors with pseudo-range and carrier phase observations on L1 and L2 frequency have been removed during the post-processing of data to obtain corrected STEC. The satellite and receiver biases have been obtained from the website: ftp://ftp.uni-be/aiub/CODE. The corrected STEC data were converted into vertical total electron content (VTEC) using the following Equation (1) given by Rama Rao *et al.* (2006):

$$\mathrm{VTEC} = (\mathrm{STEC} - |b_R + b_S|)/S(E_l), \tag{1}$$

where b_R and b_S are receivers and satellite biases, respectively, (E_l) is the elevation angle of the satellite in degrees, $S(E_l)$ is the obliquity factor with zenith angle χ at the ionospheric pierce point (IPP) and VTEC is the vertical TEC at the IPP. The obliquity factor $S(E_l)$ [or mapping function, given by Equation (2)] is defined according to a two-dimensional thin shell model at 350 km ionospheric height to define the slant and vertical TEC mapping function (Mannucci *et al.* 1993):

$$S(E_l) = \frac{1}{\cos\chi} = \left\{1 - \left(\frac{R_E \cos(E_l)}{R_E + h}\right)^2\right\}^{-1/2}, \tag{2}$$

where R_E is the mean Earth's radius in km, h is the height of the ionospheric shell above the Earth's surface, χ is the zenith angle and E_l is the elevation angle of satellite in degrees. The software tool to process the RINEX-formatted TEC data used in the present study could be found elsewhere (Seemala & Valladares 2011).

It is important to note that the error in VTEC computation from STEC could be very large for lower elevation angles due to a multipath effect, tropospheric scattering due to water vapour and so on. Therefore, to reduce this error in VTEC, only those satellite signals are considered that have high enough elevation angle (>20°). The high elevation cut-off allows only those GPS signals with IPPs at 350 km altitude and above near the ground GPS receiver. The latitudes and longitudes of IPPs have been calculated from the RINEX navigation message data by using

Table 1. Details of the selected storms and associated perturbation in geomagnetic parameters and TEC is given.

Date of storm	Date of SSC	Dst (nT)	Peak Dst local time	Maximum increase in TEC during storm period
26 September 2011 (2300 UT)	26 September (0700 UT)	−118	Night	∼22 TECU
15 July 2012 (1800 UT)	14 July (17:00 UT) and 15 July(0000 UT)	−139	Night	∼10 TECU
19 February 2014 (0800 UT)	18 February (1400 UT)	−116	Day	∼13 TECU
20 December 2015 (2200 UT)	19 December (1700 UT)	−170	Night	∼35 TECU

standard coordinate transformation formulae and corrections in satellite orbits (Hofmann-Wellenhof *et al.* 2001). The errors that affect the STEC measurements, which is then propagated to the VTEC, is directly associated with the errors in the computation of the receiver and satellite biases. The biases for the satellites and the receiver used in the present work were computed using the LaPlata Ionospheric Model (Brunini *et al.* 2008). According to Ciraolo *et al.* (2007), the mean error on the STEC should be in the order of ±3 TECU. In the rest of paper, the term TEC refers to VTEC.

The Dst index is obtained from the website http://swdcwww.kugi.kyto, and IMF B_z, solar wind velocity are downloaded from the Omni website (https://omniweb.gsfc.nasa.gov). The dawn–dusk component of the interplanetary electric field (IEF) E_y is computed using Equation (3) (Zhao *et al.* 2008):

$$E_y(\mathrm{mV/m}) = -B_z(\mathrm{nT}) \times V_x(\mathrm{km/s}) \times 10^{-3}, \qquad (3)$$

where V_x is the solar wind velocity in the Sun–Earth direction. The detailed description on geomagnetic parameters is also shown in Table 1.

3. Results and discussion

3.1 *Geomagnetic storm of 26 September 2011*

The variation of Dst index, solar wind speed, proton density, IMF B_z, IEF E_y and TEC (at Varanasi and Bengaluru) during 26–30 September 2011 is shown in top to bottom panels of Figure 1, respectively. In TEC curves, the event day TEC and mean quiet days TEC are displayed by red and blue colour, respectively. The quiet days mean TEC was computed by averaging the TEC values of five most quiet days in a given month (available at: http://wdc.kugi.kyotou.ac.jp/qddays/index.html).

It can be seen from top panel of Figure 1 that the Dst index started to turn southward at ∼1700 UT and reached the lowest value of −118 nT at ∼2400 UT. It is also observed that the IMF B_z turned southward at 1300 UT and remained in a southerly course until 1700 UT where it reached a value of −30 nT. At the same time, the values of IEF E_y vary from −6 to 6.37 mV/m (increment of 12.37 mV/m). Thereafter, IMF B_z again turned southward at ∼1800 UT and reached the lowest value of magnitude −25 nT. It remained southward until 2400 UT on 26 September. During this, IEF E_y turned eastward and changed by 15.71 mV/m (−1.37 to 14.34 mV/m). The rapid up and down recursions in IMF B_z can be easily seen from Figure 1 during 1000–1700 UT. This shows the presence of storm sudden commencement (SSC). After the SSC, the main phase of the geomagnetic storm sustained from 1700 to 2400 UT. Figure 1 also shows a sharp increase in solar wind speed and solar proton density at ∼1000 UT. The solar wind speed increased by ∼400 km/s from its initial value and solar proton density increased from 10 to 35 cm^{-1}. A sudden and large increase in the value of solar wind speed and solar proton density indicates the arrival of a shock wave (Piersanti *et al.* 2017). At 2400 UT onwards on 26 September, the Dst index started to turn northward and reached its quiet day background level on 30 September. Thus, a long recovery phase was sustained for the storm of 26 September 2011. However, a transitory behaviour of the Dst index is seen during the recovery phase wherein it showed two times southern polarity, first at ∼0600 UT on 28 September (−68 nT) and second one at ∼0300 UT on 29 September (−56 nT). The north–south oscillation in IMF B_z and Dst index is associated with an increase in the solar wind dynamic pressure that reaches ∼25 nPa (not shown here). This shows the substorm condition on 28–29 September. The pulses in the equatorial electric field are PP electric fields caused by the fluctuations in the IEF or solar wind dynamic pressure. However, Wei *et al.* (2009) suggested that the substorm process should be

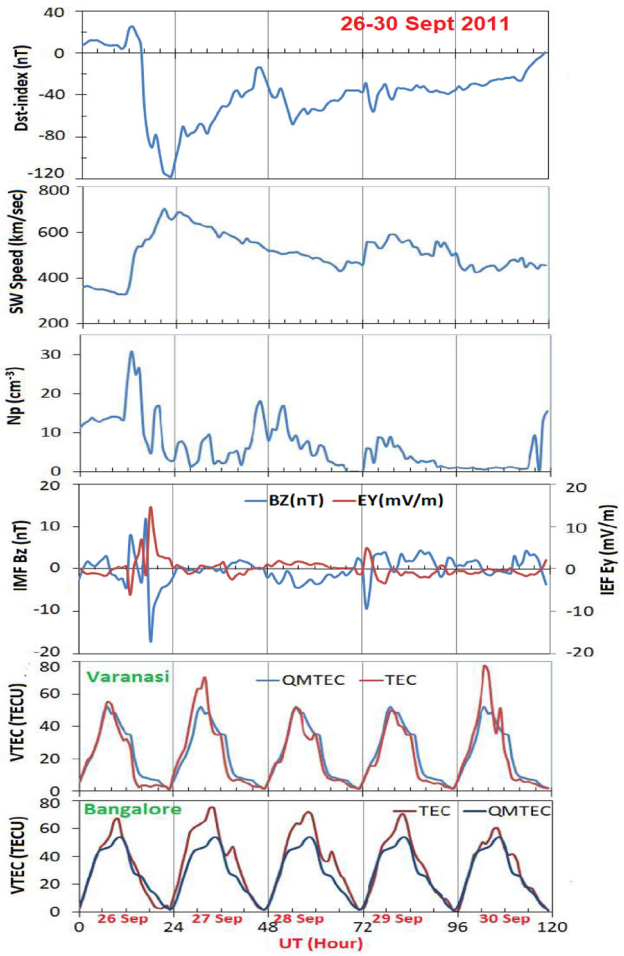

Figure 1. Variation of Dst index, solar wind speed, proton density, z-component of interplanetary magnetic field (IMF B_z), y-component of interplanetary electric field (IEF E_y) and total electron content (TEC) along with quiet mean TEC during 26–30 September 2011 is shown (from top to bottom). The TEC curve in red for an event day and blue is for quiet mean TEC.

responsible for the westward electric field through polar cap shrinkage and magnetic field depolarisation. Similar features at nearly the same time are seen in IMF B_z. It is also seen from variation of IEF E_y that the IEF E_y turned eastward and changed by 5.95 mV/m (from −1.1 to 4.85 mV/m). At this time, the IMF B_z showed a negative phase at 0100 UT on 29 September. Thus, the 26 September 2011 storm event was a triple-step development during its southerly phase that produced an intense magnetic storm in three separate regions of IMF. The possible reason may be a slow decay rate of the ring current. The variation of TEC during 26–30 September at the low-latitude station Varanasi and equatorial station Bengaluru is shown in the bottom panels of Figure 1. Figure 1 shows the increase in TEC at ∼0600 UT encompassing SSC of the geomagnetic storm. However, it is still under debate what exact mechanism is accountable for the pre-storm increase in ionospheric electron density (Danilov 2001; Liu *et al.* 2008 and references therein). A decrease in TEC of amplitude 10 TECU during 1400–2200 UT on 26 September is also observed at both the stations. At this time, the local night hours prevailed at both the stations and thus the depression in TEC is obvious due to the opposite polarity of the PP electric field and ambient field.

On 27 September, an enhancement in TEC (∼22 TECU) is observed during 0200–0800 UT at Varanasi, whereas an enhancement of ∼21 TECU is observed at Bengaluru during the whole day. It is clear from the variation of IMF B_z that it almost settled to the quiet time value. Fejer *et al.* (1979) emphasised that the prompt penetration electric fields reach the equatorial region only when IMF B_z is stable and southward. Further, Huang *et al.* (2007) have shown that the efficiency of electric field penetration to the dayside equatorial ionosphere is about 10% of IEF E_y values and will be effective when IEF E_y varies between 20 and 30 mV/m. In addition, the level of IEF E_y was also insignificant to prompt enhancement in TEC. The storm-induced wind-lifting effect may be the possible cause of the large enhancement in TEC. For this, we have checked the levels of O/N_2 on 27 September (link: http://guvitimed.jhuapl.edu), which was much higher compared to the preceding quiet day value. The storm-generated equatorward neutral winds are capable of increasing the plasma density by lifting up the ionospheric layer to higher altitudes, where the recombination loss is smaller (Rishbeth 1998). During the main phase of geomagnetic storms, the neutral winds are competent of producing up to 30% or more divergence in TEC during daytime at the middle and low latitudes (Maruyama & Nakamura 2007). On 28 September, a decrement in TEC of the magnitude 12 TECU at Varanasi during 0800–1100 UT and an enhancement of TEC of the magnitude ∼16 TECU at Bengaluru was observed throughout the day. During this time, IEF E_y is very less (2 mV/m) and such a depression in TEC at the low-latitude station Varanasi during daytime may be caused by DDEF. The effect of DDEF on the ionosphere can be felt over a timescale of a few hours to days from the storm (Scherliess & Fejer 1997; Fuller-Rowell *et al.* 2002). On 30 September, two consecutive enhancements in TEC were observed during 0600–0700 UT (∼25 TECU) and 1000–1100 UT (∼24 TECU) at Varanasi. At the equatorial station Bengaluru, the enhancements in TEC are seen during

0700–1000 (∼13 TECU) and 1400–1500 UT (∼14 TECU). Such an enhancement could be due to the storm-induced wind-lifting effect. Since the PP electric field is westward during daytime, it could not be a possible cause of the observed increase in TEC. The storm-induced equatorward neutral wind may lift the ionospheric plasma to higher altitude where recombination is smaller. This may result in enhancement in EIA peak densities (here TEC). Further, the storm-induced equatorward neutral wind in the northern hemisphere produces a large TEC enhancement than that produced by electrodynamics $E \times B$ drifts (Lin *et al.* 2005). For the September 2011 event, Wood *et al.* (2016) reported a 26% increase in global TEC from its quiet day level about 7 h after the CME reaches the Earth, followed by a decrease from a background level of 25.4–23.4 TECU, 25 h after the CME's arrival. An increase and decrease in TEC with PP and DD fields, respectively, during the 26 September event over Antarctica's American and Australian sectors have been reported by Correia *et al.* (2017). The lowest Dst value noted twice during the event reveals an intensification of a large ring current for which a large-scale IEF driven by a period of prolonged southward IMF B_z may be liable. In both cases, a sharp rise in solar wind speed affirmed the appearance of a shock in the interplanetary medium as the main phase of the geomagnetic storm events began (Kelley 2009).

3.2 *Geomagnetic storm of 15 July 2012*

Figure 2 shows variation of Dst index, solar wind speed, proton density, IMF B_z, IEF E_y and TEC during 14–19 July 2012 at Varanasi and Bengaluru stations. It is clear from Figure 2 that the main phase of 15 July 2012 geomagnetic storm was initiated at ∼0200 UT and ended by ∼1800 UT where it reached the lowest Dst value of −133 nT. After that, the recovery phase started and Dst values were levelled up to background level on 19 July. Similarly, it can be seen from variation of IMF B_z that it started to turn southward simultaneously with Dst and attained lowest values of −18 nT at ∼0600 UT. At 0600 UT on 15 July, IMF B_z also turned back to the northward direction but remained in negative phase till 0800 UT on 17 July. The variation of IEF E_y shows that, it was in just opposite phase of IMF B_z. It was east directed and its value was significantly increased by 11.45 mV/m (−0.37 to 11.08).

The TEC variation shows the enhancement of ∼20 TECU at both the stations during 0700–1200 UT on 15 July, that is a 50% increase from its quiet day level.

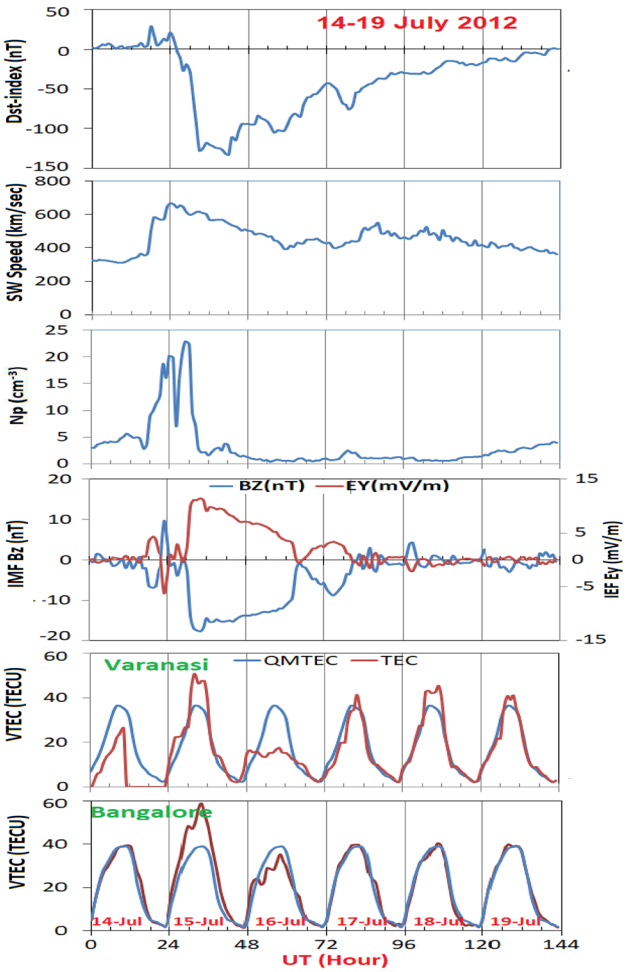

Figure 2. Variation of Dst index, solar wind speed, proton density, z-component of interplanetary magnetic field (IMF B_z), y-component of interplanetary electric field (IEF E_y) and total electron content (TEC) along with quiet mean TEC during 14–19 July 2012 is shown (from top to bottom). The TEC curve in red for an event day and blue is for quiet mean TEC.

The increase in TEC was probably associated with PP electric field as it is confirmed from the change in the value of IEF E_y during the enhancement in TEC values by an amplitude of 11 mV/m. However, there is a 3–4 h time interval to observe any disruption in the EIA vertical drift (Rastogi & Klobuchar 1990). The result of Lijo *et al.* (2011) showed seasonal dependency of the time delay that varies from 40 to 160 min. Therefore, the resulting change in TEC is seen after 40 min to 03 h. Moreover, the amplitude and latitudinal expansion of EIA is found to intensify due to the prompt penetration electric field (Lin *et al.* 2005).

On 16 July, the level of event day TEC was lower than the quiet day level during 0300–1400 UT. The amplitude of difference TEC was ∼20 TECU at

Varanasi and ∼10 TECU at Bengaluru. During this time, the IEF E_y was eastward directed and thus could not be responsible for depression in TEC. The observed decrease in TEC might be caused by the DDEF effect. The highest TEC decrement was observed at ∼0830 UT, which encompasses with noon hours at both the stations and therefore westward-directed DDEF is reasoned to be a contributing factor. This has also been reported by Liu *et al.* (2014) that the TEC time profile during the 15 July 2012 storm was the DDEF. The DDEF is westward during the daytime and can produce a downward plasma drift (Maruyama *et al.* 2004; Kumar *et al.* 2016), which results in depression in TEC. These results are consistent with Gil *et al.* (2020), wherein they observed large deviations from the average TEC behaviour over Poland on 15 July 2012.

An enhancement in TEC observed on 17 July during 0900–1000 UT at Varanasi may be caused by a neutral wind effect. On 18 and 19 July, an enhancement in TEC was observed during 0900–1100 and 0700–1300 UT, respectively, at Varanasi. These enhancements could be resulted from the storm-induced neutral wind effect. However, we do not observe significant TEC enhancements at Bengaluru during 17–19 July 2012. Chakraborty *et al.* (2015) examined the TEC variation at the Indian equatorial region, Port Blair, and EIA station Agartala during geomagnetic storms over 15–17 July 2012 and observed >50% enhanced level of TEC compared to the quiet day level at both the stations depending upon local time and phase of the storm.

3.3 *Geomagnetic storm of 19 February 2014*

The variation of geomagnetic parameters and TEC during the period 18–23 February 2014 is shown in Figure 3. The storm commenced at around 1400 UT on 18 February with the main phase onset at around 1600 UT on 18 February. The lowest southward component of Dst was −116 nT at around 0900 UT on 19 February. The decrease in Dst index is caused by an enhancement of the trapped particle population in the magnetosphere and thus by the proton ring current. After that, Dst turned northward and attained quiet time value on 22 February. Dst index showed a repeated depression on 20 February 2014 with a −60 nT at around 0600 UT and −91 nT at around 1300 UT, respectively, during its recovery phase. This may result from the superposition of two following storms provoked by two successive southward IMF

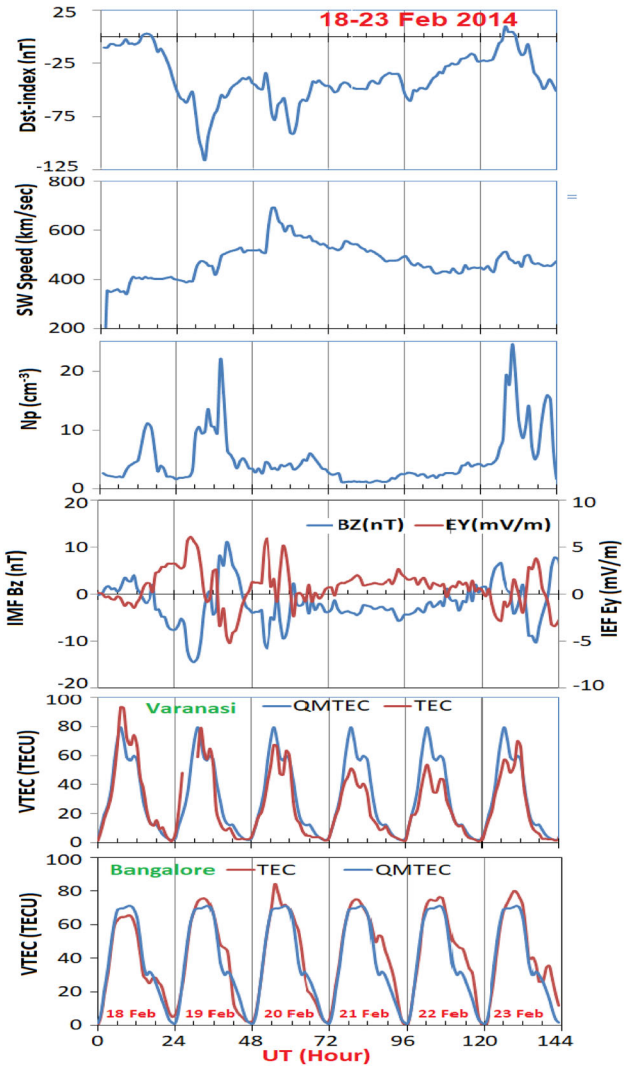

Figure 3. Variation of Dst index, solar wind speed, proton density, z-component of interplanetary magnetic field (IMF B_z), y-component of interplanetary electric field (IEF E_y) and total electron content (TEC) along with quiet mean TEC during 18–23 February 2014 is shown (from top to bottom). The TEC curve in red for an event day and blue is for quiet mean TEC.

B_z. Another cause could be that severe storms can appear from a two-step increase in the ring current, which is initially the effect of large-scale convection in the magnetosphere, and ultimately, substorm-associated injection of ionospheric O^+ ions into the inner magnetosphere (Burton *et al.* 1975). Figure 3 also shows that the IMF B_z turned southward at 1700 UT on 18 February and remained in the southerly phase till 0600 UT on 19 February. During the same time, the IEF E_y was eastward and changed by 6.29 mV/m (from 0.05 to 6.24 mV/m). The IMF B_z turned northward second time on 20 February at ∼0500 UT

and remained in the southerly phase till 1600 UT. As a result, IEF E_y turned westward and changed by −7.8 mV/m. IMF B_z attained its quiet day level at ∼0800 UT on 22 February. Figure 3 shows an enhancement in TEC during the daytime at Varanasi on 18 and 23 February. In addition, the depression in TEC is also seen during 19–22 February during daytime hours. However, for the equatorial station Bengaluru, a reduction in TEC on 18 February and enhancement during 19–23 February during daytime is observed. In a similar case, Aol *et al.* (2019) observed that the storms on 19 and 20 February 2014 inhibited the occurrence of ionospheric irregularities over Uganda. On 18 February, an enhancement in TEC over Varanasi is observed with two peaks (at 0800 and 1100 UT) encompassing the SSC (Figure 3). An enhancement in TEC during the SSC for the November 2004 storm over the Indian region has been reported by Rama Rao *et al.* (2009). The geomagnetic storm caused by a solar flare usually starts with a sudden increase of the Earth's magnetic field at the initial phase and is called an SSC. The increase in electron density during the SSC is considered to be a result of a change in the composition of the ionosphere with associated energetic particle precipitation. However, for the present case, we do not have supporting data to justify this. A careful look at the Figure 3 shows that, after recovery of IMF B_z and Dst at ∼0600 UT on 19 February, both the indexes again turned southward and remained in the southerly phase for 20–22 February. However, during its southerly phase both the parameters showed ups and down in a sequence. Thus, increase and decrease in TEC may be associated with storm-induced PP/DD electric field (Fuller-Rowell *et al.* 2002; Dashora *et al.* 2009). Using multisource data, Durgonics *et al.* (2017) have studied 19 February geomagnetic storm over the Arctic ionosphere and observed negative TEC response (depletion of 7 TECU) during day hours on 19 February and an increase in TEC of the order of 10 TECU on 20 February.

3.4 *Geomagnetic storm of 20 December 2015*

Figure 4 gives the variation of the Dst index, solar wind speed, proton density, IMF B_z, IEF E_y and TEC during 19–24 December 2015 at Varanasi and Bengaluru stations. The SSC initiated at 1700 UT on 19 December followed by its main phase started with southward turning of the Dst index at 0400 UT on 20 December. The main phase ended by

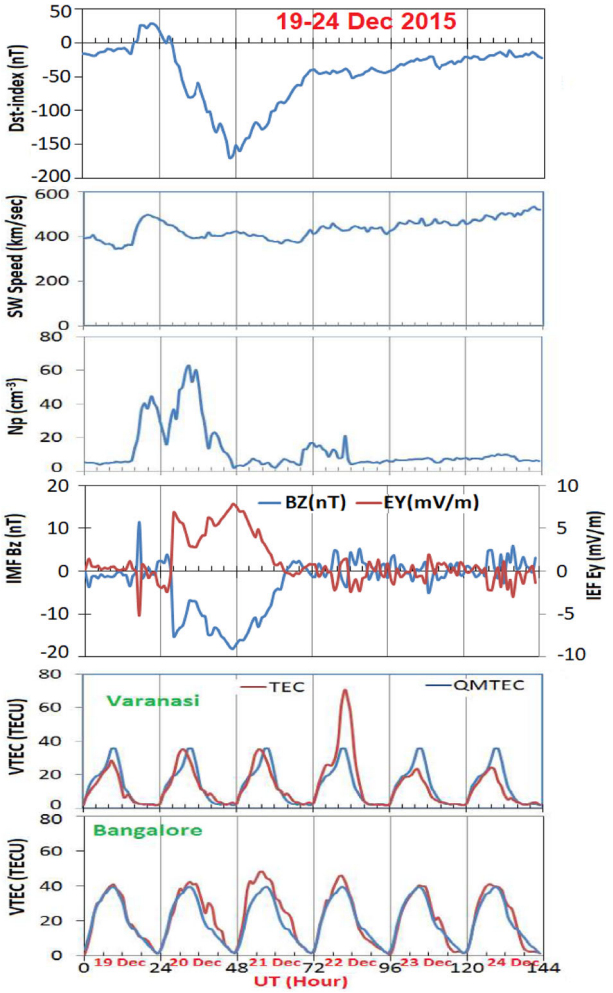

Figure 4. Variation of Dst index, solar wind speed, proton density, z-component of interplanetary magnetic field (IMF B_z), y-component of interplanetary electric field (IEF E_y) and total electron content (TEC) along with quiet mean TEC during 19–24 December 2015 is shown (from top to bottom). The TEC curve in red for an event day and blue is for quiet mean TEC.

2300 UT on 20 December where it reached down to −166 nT. Thereafter, a recovery phase of the geomagnetic storm started wherein the Dst index attained the quiet value on 22 December. The IMF B_z also turned southward at around 0200 UT on 20 December and remained in southerly phase till 2300 UT on 20 December. The IEF E_y also enhanced and changed by 10.3 mV/m (from −2.89 to 7.41 mV/m) simultaneously with IMF B_z variation. Cherniak & Zakharenkova (2018) examined the large-scale travelling ionospheric disruption during the storm main phase, with horizontal velocities of ∼700–800 m/s diffused equatorward across daytime over Europe. The present results are important to examine how low-latitude ionosphere

responded to the December 2015 event. It is easily seen from Figure 4 that the event day TEC decreased during daytime at Varanasi on 19, 23 and 24 December and showed enhancements on 20 December (∼10 TECU), 21 December (∼10 TECU) and 22 December (∼35 TECU). At Bengaluru, TEC enhancement is observed during 20–22, and on 24 December with a maximum increase on 10 TECU. In contrast, at Varanasi depression in TEC was observed during the daytime on 19, 23 and 24 December. Enhancement in TEC at both the stations during 20–21 December may be partially altered by the eastward turning of IEF E_y whereas an enhancement on 22 December may be caused by storm-induced wind-lifting effect. Because of sunlit hours prevailing on 22 December during the storm, IEF E_y was westward directed and therefore it could not have contributed to the increase in TEC. These results are consistent with the results reported by Jin *et al.* (2017) for the geomagnetic storm of March 2015. The IMF B_z turned southward at ∼0330 UT on 20 December 2015 and reached a value of about −18 nT at around 0500 UT. After that, it remained in a southerly phase till 2330 UT. Thus, the main phase of the geomagnetic storm sustained from local morning hours (LT = +0530 h) on 20 December to the next local dawn (21 December). Interestingly, the IMF B_z takes the whole day of 21 December to recover its background level. From the TEC curves it is observed that the TEC at low and equatorial station increases by ∼15 and 5 TECU during when IMF B_z was falling downward. On 21 December, when the recovery phase of the geomagnetic storm was operative, an enhancement in TEC of ∼15 TECU observed at both the stations. However, the enhancement at the equatorial station Bengaluru was more distinct. Thus, our observation shows enhancement in TEC during both the main as well as the recovery phase. Recently, Paul *et al.* (2020) have studied the ionospheric response over the low- and mid-latitudes along the 78°±3°E longitude sectors are studied for the 20 December 2015 geomagnetic storm using TEC and foF2. They observed a large TEC variation at a low- and mid-latitudes station during the main phase of the storm that was attributed to the PP electric field. On 22 December, when IMF B_z was showing a quiet day trend, unexpectedly a large increase in TEC was observed at the low-latitude station Varanasi, and a comparative less but significant increment in TEC was also observed at Bengaluru. On examining the Thermosphere Ionosphere Mesosphere Energetics and Dynamics/Global Ultraviolet Imager (TIMED/GUVI) global maps of (O/N_2) variations during 19–24 December 2015 (checked at link-http://guvitimed.jhuapl.edu/), it is clear that the (O/N_2) was significantly higher during 20–21 December compared to 19 December over the chosen stations. Thus, the observed TEC increases during both main and recovery phases of the storm are reasonably justified. Our results concerning the positive or negative storm effect in TEC with increase or decrease in O/N_2 are consistent with the results reported by Bagiya *et al.* (2011) and Chakraborty *et al.* (2015) for the cases of geomagnetic storm 17 May 2005 and 24 April 2012, respectively. However, the TIMED/GUVI map does not show comparative higher O/N_2 on 22 December; rather, it is observed to be reduced. Joule heating during the period of geomagnetic storms creates an equatorward neutral wind that transports increased molecular species. The neutral species O_2 and N_2 being heavier can reach later leading to decrease an atom to molecule ratio (O/O_2 and O/N_2) and resulted in a negative ionospheric storm effect (Rishbeth *et al.* 1987). Thus, the large increase in TEC on 22 December probably associated with local electrodynamics or storm-induced meridional winds. In the above, we have discussed four geomagnetic storm events and their impact on ionospheric TEC at chosen stations in the Indian low-latitude region. The main findings of the work are summarised as follows.

4. Summary

In this paper, we have presented the effect of intense geomagnetic storms on the variation of TEC at a low-latitude station, Varanasi, and at the equatorial station, Bengaluru, during the ascending phase of the solar cycle 24. For this, a total of four intense geomagnetic storms that occurred on 26 September 2011, 15 July 2012, 19 February 2014 and 20 December 2015 during 2010–2015 have been chosen based upon availability of TEC data. These storms are unique in terms of their long recovery phase embodied with substrom conditions (except December 2015). Our results show enhancement as well as decrements in TEC depending upon the variation of geomagnetic parameters (magnitude and polarity) and local time at given locations. The magnitude of TEC enhancements is observed to be ranging from 10 TECU to 35 TEC during different chosen

geomagnetic storms. These results are consistent with earlier work from Varanasi and Bengaluru. Kumar & Singh (2010) studied the ionospheric response to the geomagnetic storm of 20 November 2007, 9 March 2008 and 11 October 2008 using TEC at the low-latitude station Varanasi. Their study revealed enhancement in TEC of the order 15 ± 5 TECU associated with the storm-generated wind lifting and two-step enhancement of ring current. Sharma *et al.* (2011) observed the TEC enhancement by about a factor of 2 at Bengaluru during the geomagnetic storm of 24 August 2005 that attributed to the PP electric field and the abnormal plasma fountain arising from the first PP electric field. Galav *et al.* (2012) also studied the TEC response at Bengaluru to a geomagnetic storm of 30 May 2005 and reported 60% TEC enhancement. Kundu *et al.* (2020) reported 19–44% TEC changes at Bengaluru station during the selected geomagnetic storms of the years 2014–2017. Lissa *et al.* (2020) studied the response of equatorial and low-latitude ionosphere during an intense geomagnetic storm of 26 August 2018 using the TEC observations from chains of GPS stations namely Colombo, Bengaluru, Hyderabad, and Lucknow along 80°E and observed the positive storm effect during the main and recovery phases that attributed to the eastward prompt penetration electric fields in addition to the strongly enhanced ratio of thermosphere neutral composition.

Consistent with above research, results of the present work also show that the storm-induced electric field and neutral winds are the main factors for observed TEC changes during chosen geomagnetic storms. In a few cases (e.g., February 2014 and December 2015 geomagnetic storms), the low-latitude station Varanasi and equatorial station Bengaluru responded differently to the geomagnetic storm. A negative storm effect was observed at Varanasi whereas a positive storm effect was observed at Bengaluru. A large TEC change is observed during the storm main phase/recovery phase that is attributed to the PP/DD electric field depending upon the local time at chosen stations. However, a large increase in TEC at both the stations on 22 December 2015 when IMF B_z was showing a quiet trend, showed contribution from any localised electro-dynamics. In general, the increase or decrease in TEC during and after the geomagnetic storms is associated with the electric fields, neutral wind (thermospheric compositional changes) or any locally existing electrodynamics.

Acknowledgements

The work is partially supported by SERB, New Delhi, for CRG project (File No: CRG/2019/000573). The author SK is thankful to CSIR-New Delhi for providing financial assistance under Scientist Pool scheme (13(9049-A)/2019-POOL) and the author S. S. Rao is thankful to UGC-New Delhi for Dr D. S. Kothari Postdoctoral Fellowship awarded to him (vide sanction No. 4-2/2006(BSR)/ES/17-18/0048).

References

Abdu M. A. 1997, J. Atmos. Sol. Terr. Phys. 59, 1505
Aol S., Mungufeni P., Jurua E. 2019, Ind. J. Radio Space Phys. 48, 26
Bagiya M. S., Iyer K. N., Joshi H. P. *et al.* 2011, J. Geophys. Res. Space Phys. 116, AO1303
Balthazor R. L., Moffett R. J. 1997, Ann. Geophys. 15, 1048
Basu S., Basu S., Groves K. M. *et al.* 2001, Geophys. Res. Lett. 28, 3577
Basu S., Basu S., Makela J. J. *et al.* 2008, J. Geophys. Res. Space Phys. 113, A00A06
Bauske R., Noël S., Prölss G. W. 1997, Ann. Geophys. 15, 300
Blanc M., Richmond A. D. 1980, J. Geophys. Res. 85, 1669
Brunini C., Meza A., Gende M. *et al.* 2008, Adv. Space Res. 42, 737
Buonsanto M. J. 1999, Space Sci. Rev. 88, 563
Burton R. K., McPherron R. L., Russell C. T. 1975, J. Geophys. Res. 80, 4204
Chakraborty M., Kumar S., De B. *et al.* 2015, J. Earth Syst. Sci. 124, 1115
Chen W., Gao S., Hu C. *et al.* 2008, GPS Solut. 12, 33
Cherniak I., Zakharenkova I. 2018, Space Weather 16, 1377
Ciraolo L., Azpilicueta F., Brunini C. *et al.* 2007, J. Geod. 81, 111
Correia E., Spogli L., Alfonsi L. 2017, Ann. Geophys. 35, 1113
Danilov A. 2001, J. Atmos. Sol. Terr. Phys. 63, 441
Dashora N., Sharma S., Dabas R. S. *et al.* 2009, Ann. Geophys. 27, 1803
Ding F., Wan W., Liu L. *et al.* 2008, J. Geophys. Res. Space Phys. 113, 1
Durgonics T., Komjathy A., Verkhoglyadova O. 2017, Radio Sci. 52, 146
Fejer B. G., Gonzales C. A., Farley D. T. *et al.* 1979, J. Geophys. Res. 84, 5797
Fejer B. G., Jensen J. W., Kikuchi T. *et al.* 2007, J. Geophys. Res. Sp. Phys. 112, 1
Fuller-Rowell T. J., Millward G. H., Richmond A. D. *et al.* 2002, J. Atmos. Sol. Terr. Phys. 64, 1383

Galav P., Sharma S., Pandey R. 2012, Astrophys. Space Sci. 337, 543
Galav P., Rao S. S., Sharma S. *et al*. 2014a, J. Geophys. Res. Space Phys. 119, 5020
Galav P., Sharma S., Rao S. S. *et al*. 2014b, Astrophys. Space Sci. 350, 459
Gil A., Modzelewska R., Moskwa S. *et al*. 2020, Sol. Phys. 295, 135
Hahm T. S., Kulsrud R. M. 1985, Phys. Fluids 28, 2412
Hofmann-Wellenhof B., Lichtenegger H., Collins J. 2001, Global Positioning System. Springer, Vienna
Huang C. S., Sazykin S., Chau J. L. *et al*. 2007, J. Atmos. Sol. Terr. Phys. 69, 1135
Huang C. M. 2013, J. Geophys. Res. Space Phys., 118, 496
Jain A., Tiwari S., Jain S. *et al*. 2010, Ind. J. Radio Space Phys. 39, 11
Jin S., Jin R., Kutoglu H. 2017, J. Geod. 91, 613
Kelley M. C. 2009, The Earth's Ionosphere: Plasma Physics and Electrodynamics. Academic Press, Boston
Kikuchi T., Lühr H., Kitamura T. *et al*. 1996, J. Geophys. Res. Space Phys. 101, 17161
Kikuchi T., Hashimoto K. K., Nozaki K. 2008, J. Geophys. Res. Sp. Phys. 113, A06214
Kumar S., Singh A. K. 2010, Astrophys. Space Sci. 331, 447
Kumar S., Singh A. K. 2011a, Adv. Space Res. 47, 710
Kumar S., Singh A. K. 2011b, Astrophys. Space Sci. 331, 447
Kumar S., Chen W., Liu Z. *et al*. 2016, J. Geophys. Res. Space Phys. 121, 9164
Kundu S., Sasmal S., Chakraborti S. *et al.* 2020, Study the Ionospheric Total Electron Content (TEC) variation during Geomagnetic Storm in 24th Solar Cycle. 2020 URSI Regional Conference on Radio Science (URSI-RCRS), p 1, https://doi.org/10.23919/URSIRCRS49211.2020.9113605
Lijo J., Ravindran S., Vineet C. *et al*. 2011, Ann. Geophys. 29, 1267
Lin C. H., Richmond A. D., Liu J. Y. *et al*. 2005, J. Geophys. Res. Space Phys. 110, A09528
Lissa D., Srinivasu V. K. D., Prasad D. S. V. V. D. *et al*. 2020, Adv. Space Res. 66, 1427
Liu L., Wan W., Zhang M.-L. *et al*. 2008, J. Geophys. Res. 113, A02311
Liu J., Zhao B., Liu L. 2010, Ann. Geophys. 28, 795
Liu J., Liu L., Nakamura T. *et al*. 2014, J. Geophys. Res. 119, 7716
Mannucci A. J., Wilson B. D., Edwards C. D. 1993, A New Method for Monitoring the Earth's Ionospheric Total Electron Content Using the GPS Global Network. Proceedings of the 6th International Technical Meeting of the Satellite Division of The Institute of Navigation (ION GPS 1993), p 1323
Maruyama T., Ma G., Nakamura M. 2004, J. Geophys. Res. Space Phys. 109, A10302
Maruyama T., Nakamura M. 2007, J. Geophys. Res. Space Phys. 112, A05310
Mazaudier C., Venkateswaran S. V. 1990, Ann. Geophys. 8, 511
Mishra S. K., Srivastava A. K. 2019, Sol. Phys. 294, 169
Paul B., Gordiyenko G., Galav P. 2020, Astrophys. Space Sci. 365, 174
Pedatella N. M., Lei J., Larson K. M. *et al*. 2009, J. Geophys. Res. Space Phys. 114, A12313
Piersanti M., Alberti T., Bemporad A. *et al*. 2017, Sol. Phys. 292, 169
Piersanti M., Michelis P., De Moro D. D. *et al*. 2020, Ann. Geophys. 38, 703
Rama Rao P. V. S., Gopi Krishna S., Niranjan K. *et al*. 2006, Ann. Geophys. 24, 3279
Rama Rao P. V. S., Gopi Krishna S., Vara Prasad J. *et al*. 2009, Ann. Geophys. 27, 2101
Rastogi R. G., Klobuchar J. A. 1990, J. Geophys. Res. 95, 19045
Rishbeth H., Fuller-Rowell T. J., Rees D. 1987, Planet. Space Sci. 35, 1157
Rishbeth H. 1998, J. Atmos. Solar–Terrestrial Phys. 60, 1385
Sastri J. H., Ramesh K. B., Rao H. N. R. 1992, Geophys. Res. Lett. 19, 1451
Sastri J. H., Jyoti N., Somayajulu V. V. *et al*. 2000, J. Geophys. Res. Space Phys. 105, 18443
Scherliess L., Fejer B. G. 1997, J. Geophys. Res. Space Phys. 102, 24037
Seemala G. K., Valladares C. E. 2011, Radio Sci. 46, 1
Sharma S., Galav P., Dashora N. *et al*. 2011, J. Geophys. Res. 116, A05317
Srivastava A. K., Mishra S. K., Jelínek P. *et al*. 2019, ApJ 887, 137
Tsurutani B., Mannucci A., Iijima B. *et al*. 2004, J. Geophys. Res. Space Phys. 109, A08302
Vekstein G. 2017, J. Plasma Phys. 83, 205830501
Veenadhari B., Alex S., Kikuchi T. *et al*. 2010, J. Geophys. Res. Sp. Phys. 115, A03305
Wei Y., Pu Z., Hong M. *et al*. 2009, J. Geophys. Res. 114, A12209
Wood B. E., Lean J. L., McDonald S. E. *et al*. 2016, J. Geophys. Res. Sp. Phys. 121, 4938
Zhao B., Wan W., Liu L. 2005, Ann. Geophys. 23, 693
Zhao B., Wan W., Tschu K. *et al*. 2008, J. Geophys. Res. Sp. Phys. 113, A00A04